

Article

Adaptive-Energy-Sharing-Based Energy Management Strategy of Hybrid Sources in Electric Vehicles

Vishnu P. Sidharthan ¹, Yashwant Kashyap ^{1,*} and Panagiotis Kosmopoulos ^{2,*}

¹ Department of Electrical and Electronics Engineering, National Institute of Technology, Surathkal, Mangaluru 575025, Karnataka, India

² Institute for Environmental Research and Sustainable Development, National Observatory of Athens (IERSD/NOA), 15236 Athens, Greece

* Correspondence: yashwant.kashyap@nitk.edu.in (Y.K.); pkosmo@noa.gr (P.K.)

Abstract: The energy utilization of the transportation industry is increasing tremendously. The battery is one of the primary energy sources for a green and clean mode of transportation, but variations in driving profiles (NYCC, Artemis Urban, WLTP class-1) and higher C-rates affect the battery performance and lifespan of battery electric vehicles (BEVs). Hence, as a singular power source, batteries have difficulty in tackling these issues in BEVs, highlighting the significance of hybrid-source electric vehicles (HSEVs). The supercapacitor (SC) and photovoltaic panels (PVs) are the auxiliary power sources coupled with the battery in the proposed hybrid electric three-wheeler (3W). However, energy management strategies (EMS) are critical to ensure optimal and safe power allocation in HSEVs. A novel adaptive Intelligent Hybrid Source Energy Management Strategy (IHSEMS) is proposed to perform energy management in hybrid sources. The IHSEMS optimizes the power sources using an absolute energy-sharing algorithm to meet the required motor power demand using the fuzzy logic controller. Techno-economic assessment was conducted to analyze the effectiveness of the IHSEMS. Based on the comprehensive discussion, the proposed strategy reduces peak battery power by 50.20% compared to BEVs. It also reduces the battery capacity loss by 48.1%, 44%, and 24%, and reduces total operation cost by 60%, 43.9%, and 23.68% compared with standard BEVs, state machine control (SMC), and frequency decoupling strategy (FDS), respectively.

Keywords: absolute energy sharing; electric vehicle; hybrid source energy management strategy; supercapacitor; techno-economic analysis



Citation: Sidharthan, V.P.; Kashyap, Y.; Kosmopoulos, P. Adaptive-Energy-Sharing-Based Energy Management Strategy of Hybrid Sources in Electric Vehicles. *Energies* **2023**, *16*, 1214. <https://doi.org/10.3390/en16031214>

Academic Editors: Jen-Hao Teng, Kin-Cheong Sou, Alfeu J. Sguarezi Filho and Lakshmanan Padmavathi

Received: 16 December 2022

Revised: 8 January 2023

Accepted: 19 January 2023

Published: 22 January 2023



Copyright: © 2023 by the authors. Licensee MDPI, Basel, Switzerland. This article is an open access article distributed under the terms and conditions of the Creative Commons Attribution (CC BY) license (<https://creativecommons.org/licenses/by/4.0/>).

1. Introduction

In the present day, an energy predicament and environmental pollution are critical issues caused due to the acceleration in global energy demand. Expanding economy, population, and industrialization will increase India's energy demand by 2040. Energy utilization has doubled in India since 2000, 80% of which is still sourced from coal, oil, and biomass [1]. The significance of alternative sustainable and green energy sources is essential due to the exhausting resources and environmental impacts of fossil fuel energy. India's ambitions in energy policy are to reach a target of 450 GW of renewable energy by 2030, with a surplus improvement in battery energy storage and cost-competitiveness in solar PV. By 2040, India expects to have the largest battery capacity globally: 140 GW in the Stated Policies Scenario (STEPS) and 200 GW in the Sustainable Development Scenario (SDS) [2]. The intensity of emissions from India's economy is projected to improve by 40% from 2000 to 2030, and the electricity generation capacity from non-fossil fuels is expected to reach around 60% and above the Nationally Determined Contribution (NDC) of 40%. India leads in the expansion of clean energy technologies and exhibits in its market for solar PVs, wind turbines, and lithium-ion battery equipment to over USD 40 billion per year by 2040 [3]. This tremendous growth will enable India to be a highly sustainable nation with

industrial and commercial opportunities from clean energy that are even more prominent in the future.

Transportation plays a significant role in the global economy, and its energy requirement has increased tremendously to reach 29%, with massive growth in the past decade [4]. Meanwhile, the transportation industry has contributed almost two-thirds of oil demand and nearly one quarter of global carbon dioxide emissions from fuel combustion [5]. By 2050, renewable energy will occupy two-thirds of total energy consumption. By incorporating renewable electricity with electrified transportation, carbon emissions can be reduced by 60% by 2050, ensuring a sustainable and green mode of transportation [6]. For the next two decades, the energy demand for road transport is expected to double in the STEPS. Moreover, increasing numbers of two/three-wheeled vehicles directs such policies toward less energy-intensive options [7]. A shift towards electrification limits the growth in oil demand to less than 1 mb/d under the SDS [8]. In the SDS, additional capital is USD 1.4 trillion above the level in the STEPS required for clean energy technologies by 2040 [9]. India's clean energy transition lays the foundation for energy security.

The transition of transportation mode is highly essential where Lithium-ion batteries are the most widely used energy source in battery electric vehicles (BEVs) due to their higher energy density (250–400 Wh/kg), high energy efficiency (90–95%), wide operating temperature range (−20 °C–60 °C), and low self-discharge (0.5–2%) per month [10–12]. Although BEVs are developed with improved performance and comfort in mind, specific issues with lithium-ion batteries hinder their wider adoption. As per previous research, 30–50% of consumers today are interested in purchasing an EV. However, the adoption rate remains low due to various barriers. High and fluctuating C-rates (I_B/C_B), cell temperature, number of discharge and charge cycles, and depth of discharge (DOD) cause a depletion of the battery life cycle and still exist as significant issues in lithium-ion batteries [13]. The severity of these battery issues is not similar for all users and varies based on different driving and environmental conditions [14]. Battery management systems (BMS) limit such issues to an extent by monitoring and ensuring the safety of battery packs [15]. The automotive industry's strategy to increase range is with the addition of battery packs, but, in turn, this increases the weight, the need for high-power charging stations, and CO₂ emissions. The requirement for high-power charging stations is the reason why the development of charging infrastructure heavily constrains the adoption of electric vehicles. Since the battery is the single source available to handle sudden and fluctuating load demands in BEVs due to varying driving profiles, alternate strategies are necessary to ensure optimal battery operation [16].

Batteries, fuel cells, supercapacitors, and solar PVs are clean energy sources, and different combinations of these sources form the hybrid source systems in EVs. A supercapacitor (SC) coupled with a battery handles the transient load current of the EV. SC response and power density (greater than 10,000 W/kg) are higher than that of batteries (300–1000 W/kg); thus, it can ensure battery safety [17,18]. However, varying driving and environmental conditions can further affect battery life and performance. Fuel cell electric vehicles (FCEVs) are formed by the coupling of fuel cells and batteries as the hybrid source [19]. Even though FCEVs are the future of EVs, customer reliability is highly affected by the non-availability of fuel cell charging stations [20]. Countries such as Afghanistan, Argentina, Australia, the Middle East, and African countries can employ solar panels to charge EV sources during the daytime, since their conditions for solar PVs are excellent (average daily output exceeds 4.5 kW hours per installed kilowatt of capacity) (kWh/kWp) [21].

Electric vehicles utilizing hybrid sources are called hybrid-source electric vehicles (HSEVs). DC–DC converters interconnect the hybrid sources and improve the vehicle's efficiency and range. Kouchachvili et al. demonstrated a Battery–Supercapacitor vehicle with passive topology drawbacks [22]. Direct parallel connection without any converter affects each source's safety and effective utilization. Higher DC bus voltage fluctuations exist due to the unregulated DC bus adversely affecting the EV motor drive performance [23]. Nguyen et al. demonstrated an SC-controlled semi-active configuration that improves

the energy management among the battery and SC [24]. Semi-active topology affects the effective utilization of SCs, since they are directly connected to the DC bus and cause improper DC bus voltage regulation. Vargas et al. [25] and Pranoy et al. [26] demonstrated a fully active-controlled bi-directional buck-boost converter with a multi-input single-output structure. The topology enables reduced voltage ratings for the sources since the converters individually control them. Cabrane et al. presented a detailed comparison of existing topologies for hybrid sources with Battery, SC, and PV combinations [27]. A fully active topology ensures that the highest performance is utilized in hybrid-source EVs. Moreover, the allocation of power among each source plays a prime role in the system's overall efficiency. Energy Management Strategies (EMS) perform this task and ensure optimal power sharing between the hybrid sources.

EMS plays a significant role in the overall energy efficiency and performance of the HSEV. It defines the power allocation towards each source in the hybrid system, considering the vehicle and source conditions. The majority of hybrid-source EVs employ a rule-based and fuzzy-based EMS due to its ease of real-time implementation and low computational cost [28,29]. However, rule-based EMS are less adaptive to varying driving conditions but easy to implement in real-time. The major drawback of rule-based EMS is instability in applying the same algorithm to different power trains and source architectures [30]. Calibration is necessary to update the control parameters for a specified range of any driving profile [17]. The rule-based strategy's drawbacks are detailed with a battery–SC hybrid-source-based EV, where defined rules may fail to allocate the power between the sources during varying driving conditions. The battery experiences fluctuating current demands to meet varying driving profiles [31]. A low-pass or high-pass filter splits the load power demand to perform energy management among the sources. The fixed filter cuts off frequency outcomes in a less adaptive EMS in battery–SC EVs. Castaings et al. developed an EMS with a fixed frequency-multiplier rule-based strategy [32]. The fixed frequency of the filter reduces the flexibility of the system. EMS utilizes three cut-off frequencies for a battery–SC hybrid EV where the frequencies are selected based on the variations in SC_{SOC} [33]. However, fluctuating load power may result in less efficient power allocation. EMS with optimized and adaptive control variables further improve the power allocation among hybrid sources.

Dynamic EMS ensure an adaptive control of the hybrid energy management with optimized source operations. Offline optimization strategies include dynamic programming (DP) [34], particle swarm optimization (PSO) [35], and genetic algorithm (GA) [36], which achieve optimal solutions but face drawbacks in real-time implementations. However, online optimized strategies, such as Equivalent Consumption Minimization Strategy (ECMS) [37] and Model Predictive Control (MPC) [38], result in optimal outcomes based on accuracy in modelling and equivalence factor selections. Future driving profile requirements and the design of complex modelling are significant drawbacks of these strategies. AI-based Fuzzy EMS control achieves improved performance with a trade-off between optimality and ease of control [39]. Trovao et al. discuss a Battery–SC-powered three-wheeler with a fuzzy-based EMS to accomplish an effective power allocation; however, the lack of an effective DC bus voltage regulation creates a severe concern in the motor drive [40].

The proposed work presents a novel intelligent fuzzy-logic-based power allocation algorithm to allocate load power among the battery, SC, and PV in the HSEV. The state machine control (SMC) strategy [41] and frequency-decoupling strategy (FDS) [42] are discussed in the result analysis to analyze the effectiveness of the proposed EMS for a battery–SC–PV powered electric vehicle. The adaptiveness of these existing strategies to handle the effects of varying driving conditions is inadequate. The motivation behind the proposed EMS is to develop a hybrid source system that efficiently manages the variations in driving and environmental conditions. The control strategy aims to achieve flexible and reliable energy management and ensure optimal battery operation for different driving (driver, vehicle, and environmental) conditions across the globe. The strategy considers fluctuations in load current with an absolute energy-sharing algorithm. Overall,

a hybrid-source-powered EV is designed to improve energy efficiency and enhance the goal of sustainable transportation. The significant contributions of our proposed work are summarized as follows:

- Design and modelling of an Intelligent Hybrid-Source Energy Management Strategy (IHSEMS) for a Battery–SC–PV hybrid-source EV based on absolute energy sharing to ensure an effective and optimal power allocation without any complex modelling and data collection.
- Investigation of EV technical and economic parameters of proposed IHSEMS compared with BEVs and standard EMS.
- Stabilization of DC bus voltage and minimization of fluctuations during varying driving and environmental conditions.
- Contrary to the existing EMSs (SMC [41] and FDS [42]), the proposed work is highly adaptive and effective towards different driving and environmental conditions. It improves the SC utilization and reduces the RMS battery current with a downsized battery capacity, without compromising the vehicle range.

The remainder of the paper is organized as follows: Section 2 depicts the energy management system description and strategies of the proposed hybrid-source EV. Detailed parameters and the structure of each component of the system are explained in this section. The concept of the proposed energy management strategy and the technical and economic parameter evaluations are also detailed. Simulation verification and its performance assessments are included in Section 3, which investigates the importance of the proposed work, and a detailed techno-economic analysis is conducted. The paper concludes with Section 4.

2. Energy Management System and Strategies

The literature shows that optimum power allocation in the hybrid system significantly improves vehicle performance. The EMS controls the system's overall performance with reduced fuel and energy consumption [43,44], which improves battery longevity, driving range, etc. (as explained in Section 2.3), depending on the power train configuration of a hybrid source, as shown in Figure 1. The power train includes the parallel connection of pure electric sources (Battery, Supercapacitor, and PV), DC–DC and DC–AC converters, electric motor, and mechanical transmission coupled to the rear wheels.

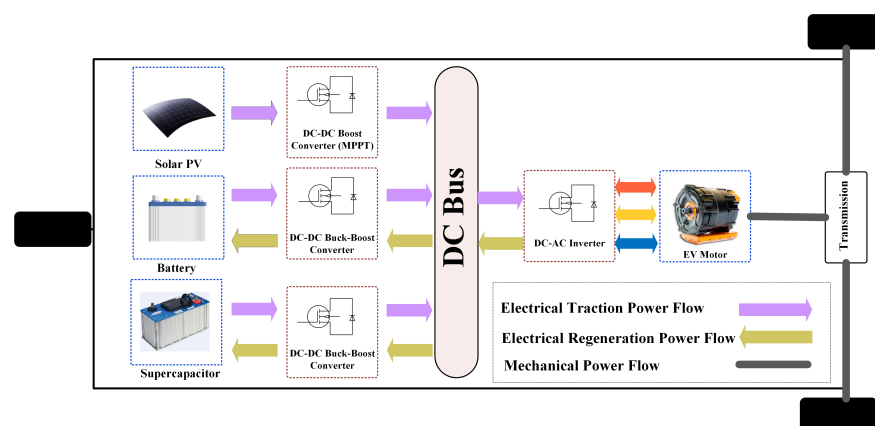


Figure 1. Power train of hybrid source system in electric 3W vehicle.

The schematic structure of a hybrid electric three-wheeler is divided into three major sections: power demand, hybrid source, and the energy management system, as shown in Figure 2. The power demand profile consists of the environment (wind velocity), driver (accelerator and brake), and load (EV motor power) conditions, as expressed in the mathematical equations (Equations (1)–(3)). A hybrid source supports the power demand profile, and the contributions of each source are detailed in Section 2.2.

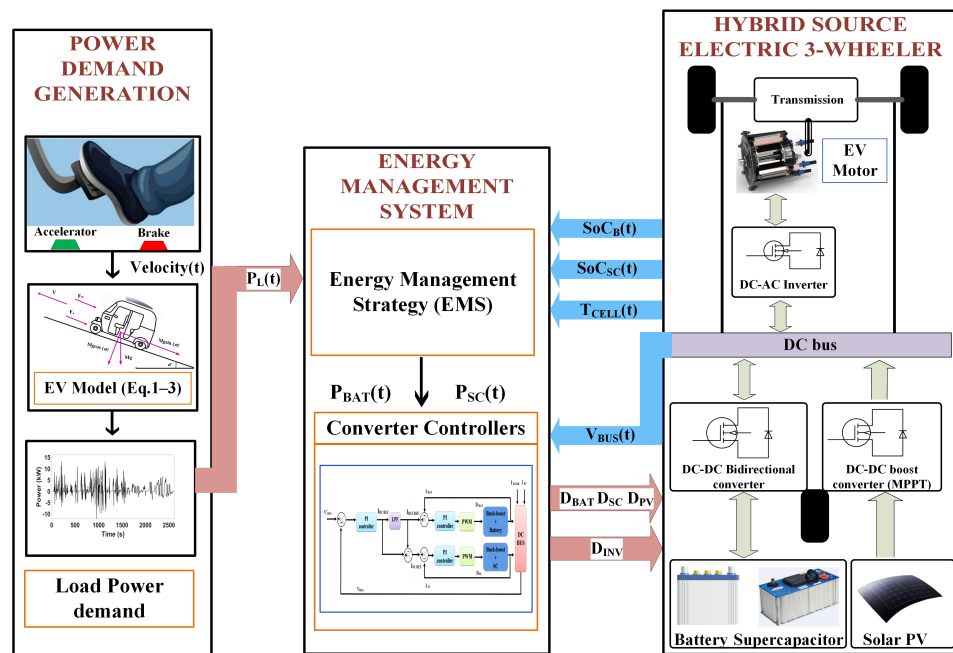


Figure 2. Schematic structure of hybrid-source energy management in electric three-wheeler.

2.1. Dynamics of Electric Vehicle

Figure 3 shows the longitudinal vehicle motion and its modeling with the dynamic equation. Table 1 shows the required parameters of an electric three-wheeler to calculate load demand [40,45]. The hybrid source supplies the required load demand estimated using a dynamic equation. The load demand during traction (P_{L1}) and braking (P_{L2}) intervals are depicted in Equations (1) and (2), respectively [44]. The P_{LT} (Equation (3)) is the total load power demand, including different resistive forces such as rolling resistance (friction on tire), aerodynamic drag (air resistance on the vehicle), and grade (opposes the motion during a road slope). These combined forces oppose the vehicle’s motion during driving and support it during braking. Moreover, the motor power overcomes the resistive force and accelerates the vehicle with the desired velocity.

Table 1. Design parameters of electric vehicle.

Sl No	Parameters	Symbols	Values
1	Vehicle category		L5M auto
2	Seating capacity		Driver + 3 seaters
3	Kerb weight	M_0	450 kg
4	Gross weight (with full capacity)	M	800 kg
5	Gradability	α	10°
6	Average velocity	V	40 km/h
7	Frontal area	A_F	2 m ²
8	Rolling coefficient	f_r	0.01
9	Drag coefficient	C_D	0.5
10	Air density	ρ	1.225 kg/m ³
11	Roof area	A_R	5 m ²
12	Acceleration due to gravity	g	9.81 m/s ²
13	Efficiency of hybrid system (%)	η_{HESS}	95
14	Transmission efficiency (%)	η_T	90
15	Motor drive efficiency (%)	η_M	85

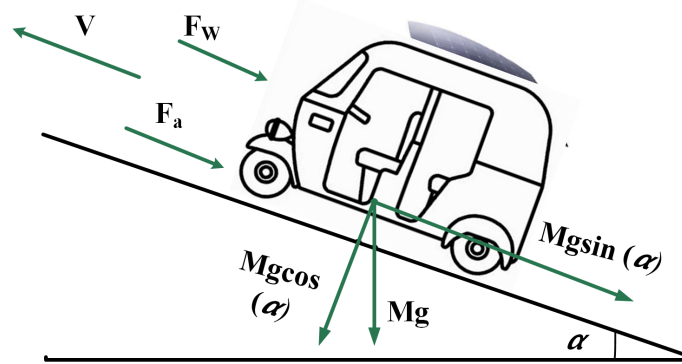


Figure 3. Dynamics of electric three-wheeler vehicle.

$$P_{L1} = \frac{\left(M \cdot g \cdot f_r \cdot \cos(\alpha) + \frac{1}{2} \cdot \rho \cdot A_f \cdot C_D \cdot V^2 + M \cdot g \cdot \sin(\alpha) + \lambda \cdot M \cdot \frac{dV}{dt} \right) \cdot V}{\eta_{HESSE} \cdot \eta_T \cdot \eta_M} \quad (1)$$

$$P_{L2} = \left(M \cdot g \cdot f_r \cdot \cos(\alpha) + \frac{1}{2} \cdot \rho \cdot A_f \cdot C_D \cdot V^2 + M \cdot g \cdot \sin(\alpha) + \lambda \cdot M \cdot \frac{dV}{dt} \right) \cdot V \cdot \eta_R \quad (2)$$

$$P_{LT} = P_{L1} + P_{L2} \quad (3)$$

where M is the gross weight of the vehicle, g the acceleration due to gravity, f_r the rolling resistance coefficient, α the gradeability, ρ the air density, A_f the frontal area of the vehicle, C_D the drag coefficient, V the velocity of the vehicle, λ the rotational inertia constant, η_R the regenerative braking efficiency, η_{HESSE} the hybrid system efficiency, η_T the transmission efficiency, and η_M the motor drive efficiency.

Standard driving profiles were used in the modeling to mimic the actual driving conditions. A combination of three standard driving profiles performs as the best test bench for any EV: NYCC (New York City cycle), Artemis Urban, and WLTP-1 (Worldwide Harmonized Light Vehicles Test Procedure). Figure 4 shows the combined driving profiles (CDP), where NYCC and Artemis Urban cycles fluctuate highly, and the WLTP class-1 cycle has fewer fluctuations [46]. This complicated CDP highlights the importance of EMS.

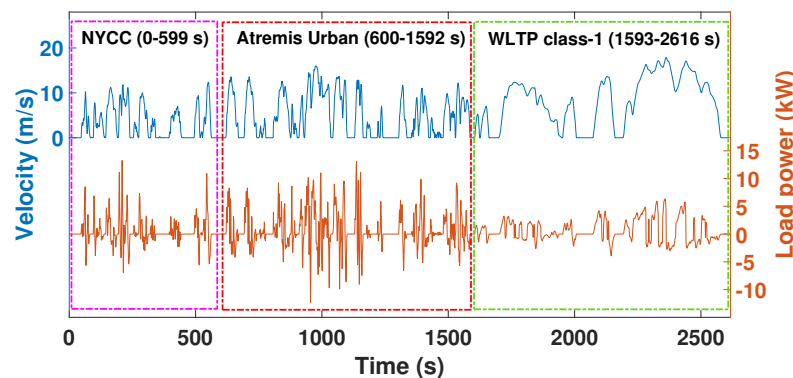


Figure 4. Velocity profile of NYCC, Artemis Urban, and WLTP class-1.

2.2. Properties of Hybrid Sources

However, the proposed work focuses on the EMS of the hybrid sources. A combination of Battery, SC, and PV are utilized as hybrid sources in the proposed HSEV. Table 2 shows the parameters of each source, and the detailed power-sharing description of each source follows in this section. The multi-input fully active bidirectional buck-boost converter interconnects the DC bus with the Battery and SC, and the DC–DC boost converter connects

the Solar PV with an MPPT control algorithm, as shown in Figure 5. EMS optimizes the battery’s energy consumption by optimizing SC and PV energy in the system. Furthermore, the ratings, weight, life, and other technical (Section 2.4) and economic (Section 2.5) parameters of the battery are compared with BEV.

Table 2. Design parameters of hybrid sources.

SI No	Components	Parameters	Values	Values
1	Lithium-ion battery	Cell type		3.2 V, 2.6 Ah, LFP cell
2		Battery capacity	C_B	5.4 kWh
3		Rated voltage	V_B	36 V
4		Specific energy	e_B	151 Wh/kg
5	Supercapacitor	Module ratings		32 V, 250 F
6		Maximum current	I_{SCmax}	1900 A
7		Specific energy	e_{SC}	3.65 Wh/kg
8	Solar PV	PV array power		965.6 W
9		Voltage at maximum power	V_{PV}	34 V
10		Current at maximum power	I_{PV}	28.4 A
11		Total panel area	A_{PV}	4.8 m ²

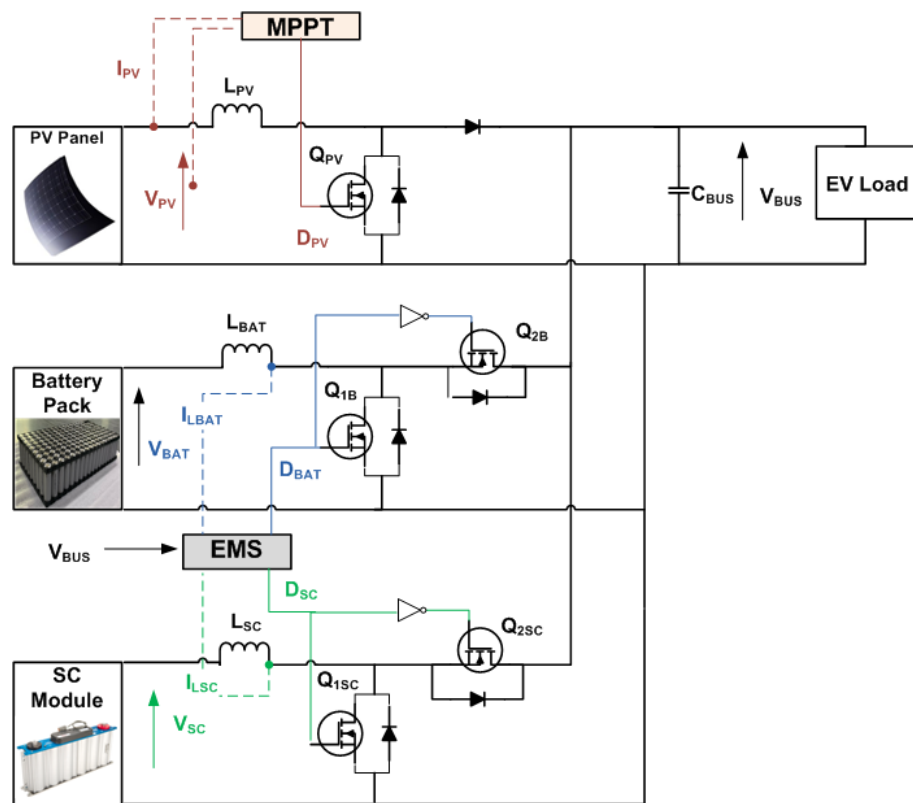


Figure 5. Circuit diagram of proposed EMS of hybrid-source electric vehicle.

Lithium-ion cells are arranged in series and parallel to achieve high energy density and ensure normal battery pack operation. An open circuit voltage (OCV)-internal resistance equivalent circuit battery model is considered in the further analysis [22,24]. The equation for battery cells and pack are as mentioned in Equation (4), [13]. Lithium-ion batteries are the primary source of the proposed EV. Table 2 shows the parameters of the lithium-ion battery pack. The battery function in the hybrid EV system is to provide a long driving

range. Due to their high energy density, batteries can support the vehicle during average power demands.

$$B_C = n_{pBc} \cdot C_{Bc}; R_B = n_{sBc} \cdot R_{Bc}/M_B; V_B = n_{sBc} \cdot V_{Bc} \quad (4)$$

where n_{pBc} and n_{sBc} represent the number of battery cells in parallel and series, B_C and C_{Bc} are the nominal capacity, R_B and R_{Bc} are the internal resistances, V_B and V_{Bc} are the voltage of the battery pack and battery cell, respectively.

The high power density of SC plays a significant role in electric vehicle applications. The SC module is designed mainly to reduce the stress of the primary source in the hybrid system (i.e., the battery) by handling sudden peak power demands and absorbing the regenerative braking energy. The proposed work combines a 12-series configuration of MAXWELL 3000F, 2.7 V cells to form the SC module. The parameters of the SC module are related to the SC cells as mentioned in Equation (5), [16]. The behavior of the SC pack can be represented by a first-order electrical element, which constitutes an open-circuit voltage (OCV), internal resistance (R_{Sc}), and capacitance (C_{Sc}). The capacitance, in parallel with an internal resistance, represents leakage of the SC model [47,48]. The parameters of SC are shown in Table 2. Due to its long life cycle (1,000,000 cycles), the degradation of SC is not considered [43].

$$C_{SC} = n_{pSc} \cdot C_{Sc}/n_{sSc}; R_{SC} = n_{sSc} \cdot R_{Sc}/n_{pSc}; V_{SC} = n_{sSc} \cdot V_{Sc} \quad (5)$$

where n_{pSc} and n_{sSc} represent the number of SC cells in parallel and series, C_{SC} and C_{Sc} are the nominal capacity, V_{SC} and V_{Sc} are the nominal voltage, and R_{SC} and R_{Sc} are the internal resistances of the SC module and SC cell, respectively.

Figure 6 shows the high fluctuating irradiance and ambient temperature environmental conditions to exhibit the system's response. Solar energy is highly recommended for electric vehicles to improve energy efficiency. Photovoltaic (PV) panels are employed to trap the solar energy. A PV array is a group of PV modules connected in series and parallel. Table 2 shows the parameters of PV panels employed in this work. The area of solar panels is selected based on the vehicle roof area as listed in Table 1 [49]. The MPPT algorithm extracts maximum power during irradiance and temperature fluctuation. PV supports the primary source battery and maintains the energy demand. The output current of the PV module is depicted in Equation (6). The PV peak power and load energy calculations of the HSEV are as follows in Equation (7) [21]. The impact of PV power is reflected in BEC_M (Equation (7)), which shows the reduction in battery energy consumption per month with the inclusion of PV panels over the vehicle, and is summarized in Table 3.

$$I_{PV} = n_p \cdot I_{PH} - n_p \cdot I_{RS} \cdot \left[\exp \left(\frac{V_{PV} + I_{PV} \cdot R_S}{V_{TH} \cdot n_s} \right) - 1 \right] - \frac{(V_{PV} + I_{PV} \cdot R_S)}{R_{SH}} \quad (6)$$

where V_{PV} and I_{PV} represent the output PV voltage and current of the module, n_p and n_s are the number of parallel and series connected panels. I_{PH} is the photo-current, I_{RS} is the module reverse saturation current, V_{TH} is the diode thermal voltage, and R_S , R_{SH} are the series and shunt resistance, respectively.

$$W_P = \frac{I_r \cdot A \cdot \eta_{PV}}{100}; LEC_{Day} = EC_{Dc} \cdot N_{Dc}; BEC_M = TEC_M - E_{PVM} \quad (7)$$

where W_P is the installed peak PV panel power, η_{PV} is the PV conversion efficiency, LEC_{Day} represents the load energy consumption per day, EC_{Dc} is the energy consumption per driving cycle, N_{Dc} is the number of driving cycles needed to complete the total expected drive per day, and BEC_M , TEC_M , and E_{PVM} are the battery energy consumption, total energy consumption, and PV energy consumption per month, respectively.

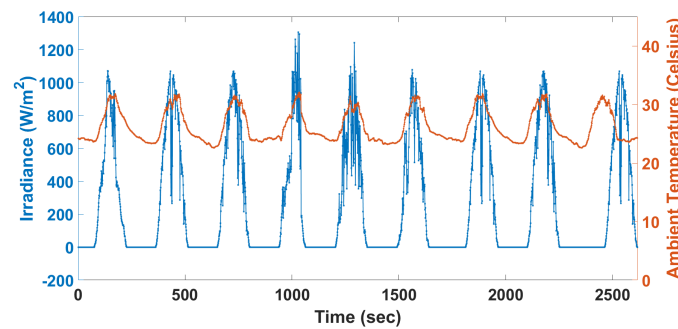


Figure 6. Irradiance (blue), ambient temperature (red).

Table 3. Cases of electric vehicle drive.

Sl no	Parameters	Case-I	Case-II	Case-III
1	Daily energy demand (Wh)	3445	3445	3445
2	Monthly energy demand (Wh)	124,020	124,020	124,020
3	Monthly PV energy generation (Wh)	63,600	31,800	0
4	Monthly battery energy consumption (Wh)	60,420	92,220	124,020
5	Daily 3W EV drive distance(km)	100	100	100
6	Daily PV range (km)	60	30	0

2.3. Proposed Energy Management Strategy

This section examines the challenges in several EMS approaches. A hybrid-source system follows the deterministic rule-based strategy for ease in real-time operation, which limits the source performance [50]. The vehicle needs an adaptive and flexible control strategy under varying driving conditions. If EMS does not take the driving profile and source parameters into account, this may lead to an unstable system. This affects the battery's performance and life, as mentioned in Section 2.4 on the technical and Section 2.5 on the economic aspects. The two standard EMS, (1) SMC [41] and (2) FDS [42], illustrate the significance of the proposed EMS. The SMC includes eight states to control energy management using hysteresis switching, which delays the system's response during sudden load changes [41]. The FDS performs the energy management by providing low-frequency load demands to the battery and high frequency to SC using a fixed-frequency low-pass filter, which reduces adaptivity and flexibility during varying driving conditions [42]. A more detailed comparison of EMS is given in Section 3.2.

The proposed EMS ensures each source's effective utilization by considering the impact of varying driving conditions. The energy generated from each source is used in the algorithm and allocated in an optimal ratio to meet load power demand. The main optimization parameter is the absolute energy of low- and high-frequency components. The present research highlights the significance of the proposed absolute energy sharing scheme (as in Equations (12) and (13)). The variation in low- and high-frequency absolute energy is monitored throughout the driving cycle. The control algorithm is assigned to modify the energy management ratio between the sources. An intelligent fuzzy logic strategy enables absolute energy sharing of sources as membership functions; therefore, it is named an Intelligent Hybrid-Source Energy Management System (IHSEMS). The function of the proposed EMS is not limited to hybrid-source energy management; moreover, it maintains SC_{SOC} , as mentioned in Section 3.2.1. The proposed EMS improves the EV's long-term economy by providing the SC throughout the driving cycle and reducing battery capacity losses and stress.

The fuzzy control strategy makes the control process more realistic and particularly suitable for controlling nonlinear systems [50]. An intelligent fuzzy logic control strategy improves the battery's range, performance, safety, and life cycle. The proposed control strategy focuses on monitoring the charging levels (source conditions), load current fluctuations (driving conditions), maximum current (C-rate), and irradiance (environmental

conditions), and creates an optimum cut-off frequency for the low-pass filter to ensure an effective power-sharing strategy. In EVs, the load current continuously varies. Fuzzy logic works to split the combined power P_C between the battery and SC while changing the cut-off frequencies. The fuzzy system consists of four inputs and one output parameter: the low-frequency absolute energy ($Abs E_{LF}$), high-frequency absolute energy ($Abs E_{HF}$), SC state of charge (SC_{SOC}), battery cell temperature (T_C) and the cut-off frequency (F_{CUTOFF}), respectively. Further, the above fuzzy parameters are defined into three membership functions: Low, Medium, and High, as shown in Figure 7.

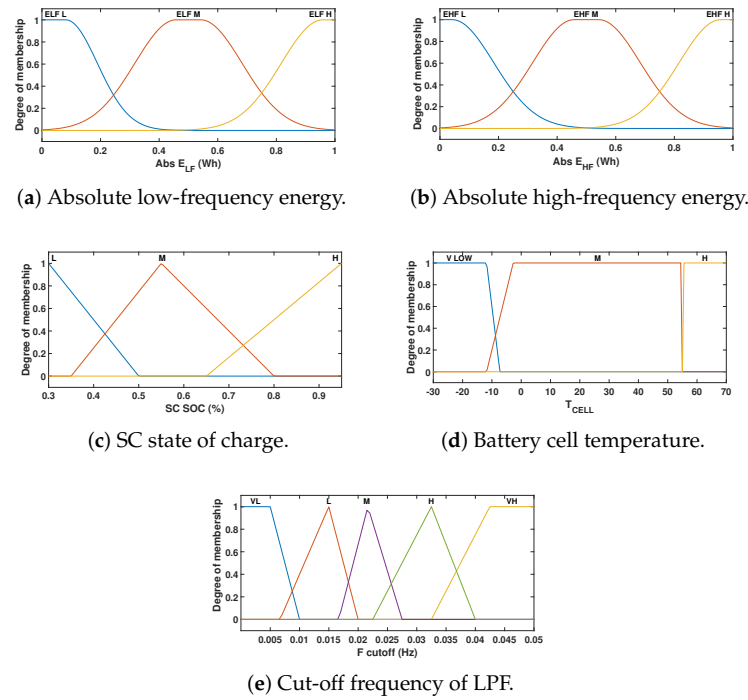


Figure 7. Input and output membership functions of fuzzy controller.

IHSEMS allocates the load power among each source based on various driving conditions. Equation (8) explains the total power handled by the hybrid sources.

$$P_T = P_B + P_{SC} + P_{PV} = P_C + P_{PV} = P_{LT} \tag{8}$$

where P_T is the total power from hybrid sources, P_B , P_{SC} , and P_{PV} are battery, SC, and PV power, respectively, and P_C is the combined power of the battery and SC. Equation (9) shows the battery's and SC's combined power.

$$P_C = P_B + P_{SC} = P_{LT} - P_{PV} \tag{9}$$

The adaptive low-pass filter (LPF) separates the load fluctuations into low and high reference currents. The battery and SC handle low (steady-state) and high (transient) frequency load current, respectively, as shown in Equation (10). The total current supplied from hybrid sources is shown in Equation (11).

$$I_{LF} = I_C \cdot \frac{(2 \cdot \pi \cdot f_c)}{(s + 2 \cdot \pi \cdot f_c)}; I_{HF} = I_C - I_{LF} \tag{10}$$

$$I_T = I_{LF} + I_{HF} + I_{PV} \tag{11}$$

where, I_{LF} , I_{HF} are low-frequency and high-frequency current, f_c is the cut-off frequency of LPF, I_C is the total current demand and I_T is the sum of current from the battery, SC, and PV to meet the load current.

Equation (12) explains the absolute energy of low- and high-frequency currents. Abs (E_{LF}) and Abs (E_{HF}) are the absolute energy generated by the battery and SC, respectively. The fuzzy controller limits the cut-off frequency considering the source and load conditions to satisfy an effective absolute energy sharing between the sources. This sustains the SC’s participation (the SC handles the high-frequency power) during sudden peaks, fluctuating power, and regenerative braking energy intervals. The absolute energy of the high-frequency component is higher than the low-frequency components of the load power, as shown in Equation (13). The flowchart of the absolute energy sharing algorithm is explained in Figure 8, where the cut-off frequency optimizes the energy sharing among each source, considering the fluctuations in driving and source conditions.

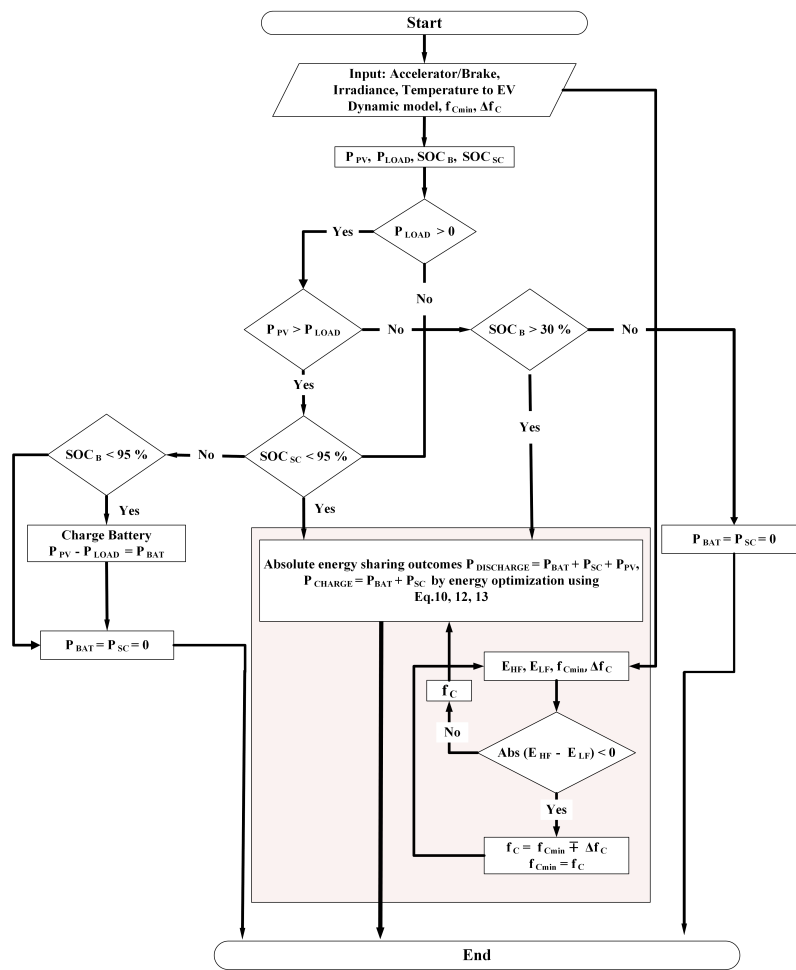


Figure 8. Flowchart of absolute energy-sharing algorithm.

$$Abs(E_{LF}) = Abs(\int (P_{LF})dt); Abs(E_{HF}) = Abs(\int (P_{HF})dt) \tag{12}$$

$$Abs(E_{HF}) - Abs(E_{LF}) > 0 \tag{13}$$

where P_{LF} and P_{HF} are the low- and high-frequency load power components.

As shown in Figure 2, the controller consists of the outer voltage and inner current control loop for the battery and SC, which satisfies the battery’s and SC’s dynamics. The inner SC current loop operates faster than the outer voltage control loop to ensure the stability of the overall control system [42]. The outer voltage loop operates to stabilize constant DC bus voltage [27]. The IHSEMS generates the reference power for each source and utilizes a controller to generate the switching pulses required for the DC–DC converters. Thus, the IHSEMS ensures efficient power flow respective to absolute energy sharing. The

PI controllers of each loop provide the desired phase margin at the required bandwidth for ensuring system stability based on frequency domain specifications [42]. The small-signal modelling (SSM) of the converter system generates PI values of each controller loop using the MATLAB SISO tool [51]. PI controllers reduce the error of reference versus actual source current. PWM derives the duty ratio for converters and generates the switching pulses for each converter D_B and D_{SC} . The P&O MPPT algorithm generates switching pulses for the PV boost converter [27].

2.4. Technical Evaluation

- (a) Battery peak power reduction (B_{PPR}): The peak battery power demand (B_P) increases the battery C-rates (I_B/C_B) and reduces the life (Equation (22)) [13,44]. The percentage reduction in battery peak power is expressed as follows:

$$B_{PPR} (\%) = \left(\frac{B_P - B_{PEMS}}{B_P} \right) \cdot 100 \quad (14)$$

where B_{PEMS} is the peak battery power with hybrid EMS. The EMS ensures optimal battery operation to enhance the longevity of the battery cells. Battery downsizing (reduction in battery size) is possible by reducing the peak power demand by employing the suitable EMS [52].

- (b) Battery capacity reduction (B_{CR}): Describes the percentage reduction in battery capacity (B_C) [52].

$$B_{CR} (\%) = \left(\frac{B_C - B_{CEMS}}{B_C} \right) \cdot 100 \quad (15)$$

where B_{CEMS} is the battery capacity of Hybrid EMS. Reduction in battery capacity could be achieved by utilizing SC and PV as hybrid sources in HSEV to share the power demand.

- (c) Battery di/dt reduction (B_{IR}): Rate of change of battery current (di/dt) and the percentage reduction are expressed in Equations (16) and (17), respectively, which determines the stress on the battery.

$$di/dt (A/s) = \frac{I_{max} - I_{min}}{t_{max} - t_{min}} \quad (16)$$

$$B_{IR} (\%) = \left(\frac{di/dt_{BEV} - di/dt_{EMS}}{di/dt_{BEV}} \right) \cdot 100 \quad (17)$$

where I_{max} and I_{min} are the maximum and minimum battery current. T_{max} and T_{min} are the respective time instants of maximum and minimum battery current. di/dt_{BEV} and di/dt_{EMS} are the di/dt ratio of BEVs and EMS, respectively. Battery internal stress directly depends on the C-rates and the battery's current fluctuation rate [53]. Higher and sudden variations in battery current cause the development of Li^+ concentration, and more non-uniform and steeper gradients in the film [54].

- (d) Battery RMS current reduction (B_{RIR}): Battery RMS current reduction % can be calculated using Equation (18), and its reduction extends the battery life [30]. RMS current is a vital factor that affects battery life and gives a rough estimation of the battery ohmic losses [55]. The system's overall losses and efficiency highly depend on the RMS current. B_{RIR} , by employing the suitable hybrid source in EVs, decelerates battery capacity degradation.

$$B_{RIR} (\%) = \left(\frac{B_{RI} - B_{RIEMS}}{B_{RI}} \right) \cdot 100 \quad (18)$$

where B_{RIR} is the battery RMS current reduction percentage, B_{RI} is the battery RMS current and B_{RIEMS} is the battery RMS current with EMS.

- (e) Battery capacity loss (B_{CL}): Instantaneous battery capacity loss, battery capacity loss, and total capacity losses are evaluated with Equations (19)–(21), respectively [44,56].

$$B_{\delta Q_{loss}(k)} = 9.78 \times 10^{-4} \cdot \left(\frac{Abs(I_{B,k}) \cdot T_s \cdot \exp \frac{(-15162 + 1516 \cdot C_{rate,k})}{(0.849 \cdot R \cdot T)}}{3600} \cdot Q_{loss,(k-1)}^{-0.1779} \right) \quad (19)$$

$$B_{Q_{loss}} = F(C_{rrate} \cdot T \cdot A_h \cdot N \cdot DOD) = B(C_{rate}) \cdot \exp p \frac{(-E_a(C_{rate}))}{(R \cdot T)} \cdot (A_h(N))^z \quad (20)$$

$$B_{Q_{loss}(k)} = 0.0032 \cdot \exp \left(\frac{(-15162 + 1516 \cdot C_{rate}(k))}{R \cdot (T + 273)} \right) \cdot Ah(k)^z; \quad (21)$$

where I_B is the battery current, T_s is the sampling interval, $B_{\delta Q_{loss}}$ is the instantaneous battery capacity loss, $B_{Q_{loss}}$ is the battery capacity loss, R is the gas constant (J/mol K), T is the absolute temperature (K), A_h is the Ah-throughput, z is the power-law factor (0.828), C_{rate} is the battery charge/discharge rate, and DOD is the battery depth of discharge.

The capacity loss of a lithium-ion battery determines the life of the battery. Reduction in capacity from the initial capacity (100%) must be less than 20% to achieve optimal battery operation for EV applications. The end of life (EOL) of a battery is defined as whenever the battery capacity reaches less than 80% of its initial capacity [57]. The Arrhenius degradation model [58] is used to depict the battery degradation, and the model explains how the battery temperature, depth of discharge (DOD), current rate C_{rate} , RMS current, and BIR (di/dt) highly deteriorate the battery life and increase the BDC Equation (28) [13,30].

- (f) Battery lifespan (B_{LS}): The significant impact on battery life is due to the battery capacity loss, as expressed in Equation (22) for a lithium-ion battery [44].

$$B_{LS} = \left(\frac{20\%}{Q_{lossD} \cdot D_{day} \cdot 365} \right) \quad (22)$$

where Q_{lossD} is the capacity loss at each distance and D_{day} is the average traveled distance per day. The highly fluctuating NYCC cycle was selected to analyze extreme battery degradation and life. However, the present analysis thoroughly studied EV battery LS for different hybrid EMS versus BEVs under uniform environmental conditions. In a Li-ion battery, if the capacity loss exceeds 20%, or the capacity goes below 80% of the nominal capacity, it is unsuitable for EV application. Battery lifespan improvement (BLSI) derives the battery life extension for the hybrid EMS compared to BEVs.

- (g) DC bus voltage fluctuations (DC_{BVF}): Equation (23) expresses the percentage variation of the peak-to-peak DC bus voltage fluctuation [27] as follows:

$$DC_{BVF} (\%) = \left(\frac{V_{max} - V_{min}}{V_{bus}} \right) \cdot 100 \quad (23)$$

where V_{bus} is the DC bus voltage and V_{max} and V_{min} are the maximum and minimum DC bus voltage. The difference gives the peak-to-peak value of the bus voltage. DC bus voltage fluctuations have severe impacts on the EV motor performance [23]. The difference between the maximum and minimum DC bus voltage gives the peak-to-peak value of the bus voltage. DC–DC converter with optimal EMS ensures a stabilized DC bus voltage.

- (h) Optimum battery size (B_{OS}): The battery size provides a standard driving range to run a vehicle without PV irradiance for a day. The n_{sBc} and n_{pBc} are selected as 10 and 58, respectively, to meet the required average power demand and nominal voltage.

$$B_{OS, n_{sBc} \cdot n_{pBc}} \geq \frac{(\rho \cdot A_f \cdot C_D \cdot V^2 + 2 \cdot M \cdot g \cdot f_r) \cdot D}{2 \cdot \eta_{HESS} \cdot \eta_T \cdot \eta_M \cdot 3600 \cdot C_{Bc} \cdot V_{Bc} - (2 \cdot M_{Bc} \cdot g \cdot f_r)} \quad (24)$$

where D is the minimum EV driving range in km and M_{Bc} is the mass of the battery cell in kg.

The battery size of HSEVs can be reduced by 26.72% compared to BEVs available in the market, as shown in Table 2. The derived battery size from Equation (1) and expressed in Equation (24) would provide the standard driving range even under adverse conditions. Additionally, the proposed vehicle can accommodate a PV panel. The output power ratings of PV are analyzed analytically in Section 3.1, considering different weather conditions.

- (i) Battery State of charge (B_{SOC}): Charge levels in the battery are decided by the SOC. Improvement in energy economy is reflected in the battery SOC levels.

$$B_{SOC} = B_{SOC0} - \int \frac{I_B}{B_C} \quad (25)$$

where B_{SOC0} is the initial battery SOC and I_B and B_C are the battery current and capacity.

- (j) SC State of charge (SC_{SOC}): SCs operate with higher efficiency at higher SOC. In order to achieve a better SC performance, SOC should not go below 40% and over 100%. The relationship between SC_{SOC} and voltage is shown in Equation (26) [14].

$$SC_{SOC} = (U_{SC}/V_{SC})^2 \quad (26)$$

where U_{SC} and V_{SC} are the working voltage and nominal voltage of the SC module, respectively.

- (k) PV range (PVR): As per the Indian electric 3W standard test case, the average driving range is 100 km per day [59]. PV energy per day directly impacts both the range and battery energy savings.

$$PV_{Range} = \frac{E_{PVday}}{ECR} \quad (27)$$

where ECR is the energy consumption rate in Wh/km, E_{PVday} is PV energy per day in Wh and PVR is the total PV range.

2.5. Economy Evaluation

- (a) EV Battery degradation cost (BDC) is the measure of battery replacement and maintenance cost from its capacity and instantaneous capacity loss (Equation (19)) [44,60].

$$BDC = \frac{B_C \cdot V_B \cdot Price_{BAT} \cdot B_{\delta Q_{loss}(k)}}{(1000) \cdot (0.2)} (INR) \quad (28)$$

- (b) EV Electricity cost (EC) is the cost associated with energy utilized (E_{source}) during the battery's charging. EC depends on the per unit cost (kWh), the battery size (Ah), and SOC (%) as expressed below [61]:

$$EC = \frac{E_{source} \cdot Price_{kWh}}{(1000)} (INR) \quad (29)$$

- (c) EV Total operation cost (TOC) describes the cost associated with battery degradation with time and energy usage. The battery degradation cost (BDC) and electricity cost (EC) of EVs determine the total operation cost of the vehicle.

$$TOC = BDC + EC(INR) \quad (30)$$

where $Price_{BAT}$ is the per-kWh battery price in India, $Price_{kWh}$ is the average price of electricity cost per kWh, B_C is the battery capacity, and V_B is the battery voltage. $B_{\delta Q_{loss}}$ is evaluated with Equation (19).

3. Results and Discussions of EMS

The proposed energy management system (Section 2) of the HSEV disengages the battery from the effects of driving conditions, whether (1) vehicle-related (acceleration, deceleration, braking), (2) driver-related (driving pattern, route planning), or (3) environment-related (temperature, irradiance, wind, road terrain) factors. Hence, it improves the battery's longevity and avoids frequent battery replacement or maintenance [62].

The proposed IHSEMS are detailed in this section with the outcomes that manage the effective power allocation among the hybrid sources for varying CDP. Table 4 assesses a detailed comparison between the IHSEMS versus BEVs, SMCs, and FDS. In this work, an electric three-wheeler exhibits the significance and effectiveness of IHSEMS. Figure 4 shows an NYCC, Artemis Urban, WLTP class-1 CDP that serves to test the IHSEMS, since their driving conditions match with the three-wheeler's average velocity. The average velocities and distances covered by each profile were 11.4 km/h and 1.90 km (NYCC), 17.7 km/h and 4.874 km (Artemis Urban), 25 km/h and 8.091 km (WLTP class-1), respectively. The following initial conditions for the initial $B_{SOC0} = 50\%$, and $SC_{SOC} = 86\%$, were considered for testing. The PV irradiance and temperature remain highly fluctuating to indicate the varying environmental conditions. The conversion efficiency of the PV panels was selected at 20% as per the availability in the market [4,63]. IHSEMS allocated the power among the battery, supercapacitor, and solar PV and was implemented in a MATLAB/Simulink environment. Moreover, the effects of variation in solar irradiance were mitigated by the SC and regulated the bus voltage with reduced fluctuations, as discussed in Section 3.1. In Section 3.2.1, the technical, and in Section 3.2.2, the economic parameters are detailed, along with their impact on the driving conditions of EVs [14].

Figure 9 shows the absolute energy sharing of battery, SC, and PV energy towards the load energy demand. Energy sharing among each source ensures that the SC is available throughout the vehicle journey to handle the high-frequency load and regenerative energy. IHSEMS manages the energy, assigning the SC with higher absolute energy and ensuring maximum utilization at any driving condition considering the SOC. Therefore, the system adaptively varies the power allocation, such as low-fluctuating highway drive and high-fluctuating city drive. An absolute energy-sharing algorithm reflects the impact and ensures the stress-free and optimal battery operation of the HSEV.

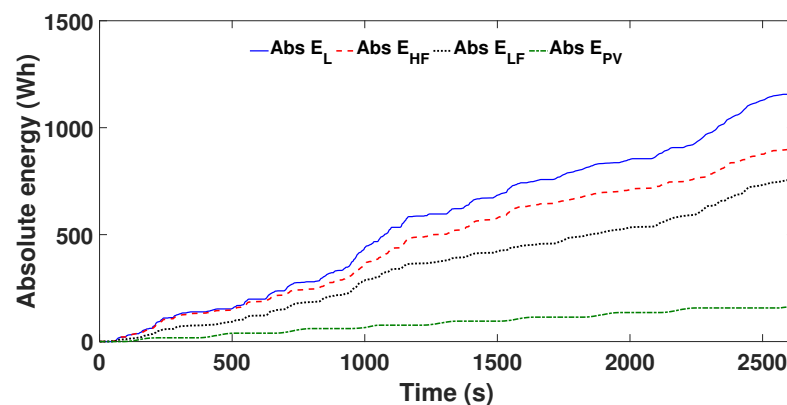


Figure 9. Absolute energy sharing profiles.

Figure 10 describes the load power versus cut-off frequency adaption. The cut-off frequency and load power for the CDP were analyzed to show the significance of the

proposed IHSEMS. NYCC and Artemis Urban cycle show city driving cases with higher load fluctuations due to traffic conditions. Since the load fluctuations are higher during the NYCC and Artemis Urban cycles, the cut-off frequency was optimized to ensure SC energy availability, and the battery achieved optimal operation throughout the cycle. The SC managed the sudden and peak load power demands in this driving interval and thus, in return, ensured a safe battery operation. The lower cut-off frequency was seen during the WLTP class-1 cycle, where the fluctuation was low compared to the other two cycles. The battery could manage such low fluctuations with the selected cut-off frequency, and the SC was used for the subsequent high-fluctuating driving intervals. Figure 10 shows a reduced cut-off frequency during the WLTP cycle to satisfy the energy optimization condition (Equation (13)) for varying driving conditions.

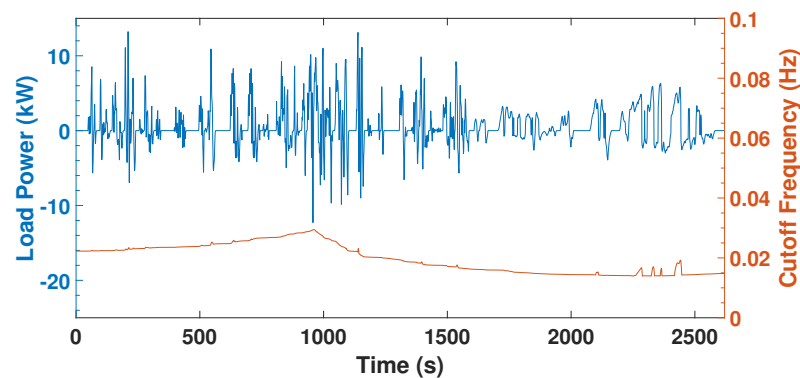


Figure 10. Cut-off frequency derived for the CDP.

The primary task of IHSEMS is to ensure optimal power allocation among each source, as shown in Figures 11 and 12. Figure 11 shows the battery discharge power remained under 5 kW throughout the driving period. The SC handled peak load power during $t = 212$ s, 1140 s, which helped to drop the battery C-rates. Most of the regenerative energy [time = 1130 s–1160 s, 2275 s–2375 s] was absorbed by the SC, which reduced the battery's recurring charge and discharges to extend its life. Figure 12 shows the energy sharing of the proposed IHSEMS where the SC energy is reserved for transient load conditions throughout the CDP based on the varying driving conditions. Moreover, the battery contributed more to smooth energy consumption during time the interval $t = 2200$ s–2500 s (under WLTP class-1) by assigning the SC to handle even minor fluctuations in the load demand, as shown in Figure 12. Overall, smooth battery energy consumption enables the stress-free operation of the battery during a sudden fall or rise in PV power.

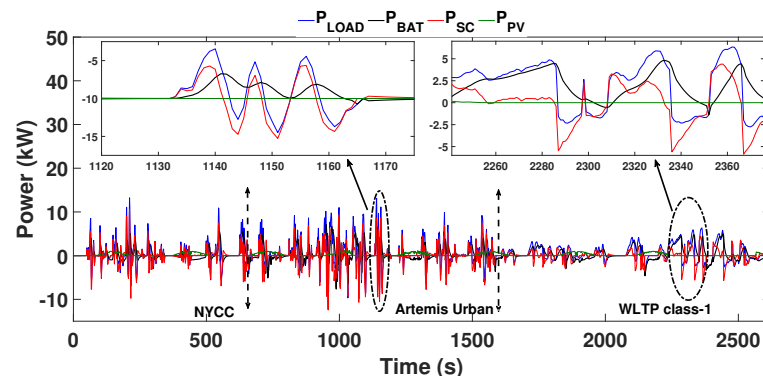


Figure 11. Comparison of battery, SC, PV, and load power (BEV) with IHSEMS.

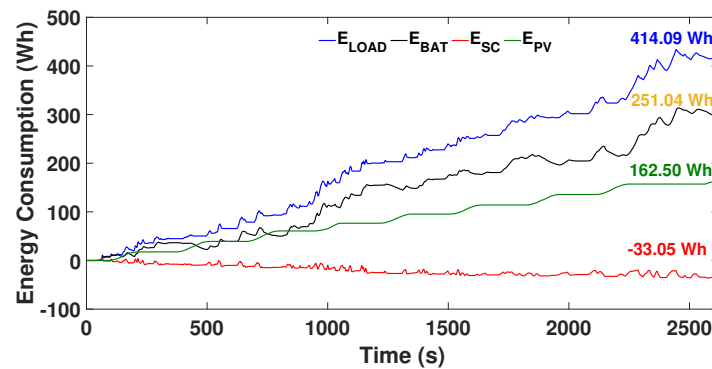


Figure 12. Comparison of source energy consumption of IHSEMS under CDP.

3.1. Impact of PV Power

PV energy is chosen based on energy consumption from actual locations with real environmental conditions. Figure 13a,b show the map of the selected location for analysis (Bangalore-12.9716° N, 77.5946° E) and the monthly PV energy generation of Bangalore (India) throughout the year, respectively [64]. The PV energy generation considers an installed peak PV power [Wp] of 965.6 W (Equation (7)) for an area of 4.8 m² [49,64]. It is evident from Figure 13b that PV energy generation is highest during March (143.63 kWh) and lowest during November (103.12 kWh). The yearly average PV energy production at Bangalore is 1455.07 kWh under a fixed panel arrangement. However, PV energy consumed by vehicles is significantly lower due to the shading on roads and parking spaces which reduces solar irradiance. Centeno et al. (2021) reported the annual average irradiance loss of 20% and 50% during driving and parking due to shading, respectively [65]. Three cases with different PV irradiance and vehicle drive conditions were examined to show the significance of PV energy in HSEV. Scheduling of the daily NYCC driving cycle of electric 3W energy management is shown in Table 3. The daily standard 100 km driver's driving cycle needs to drive 53 times that of the NYCC driving cycle [44].

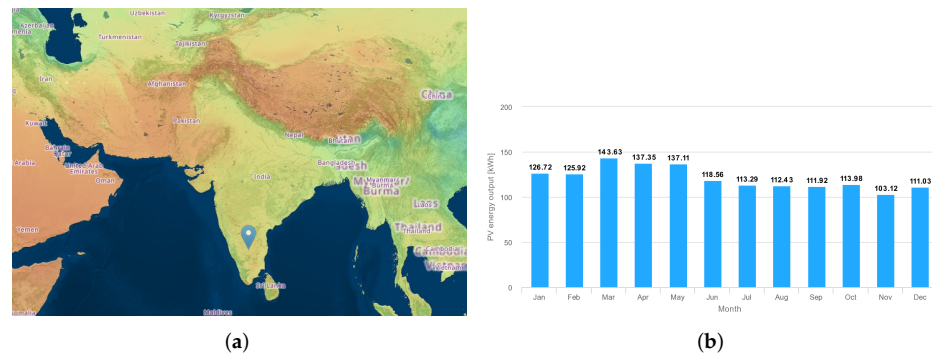
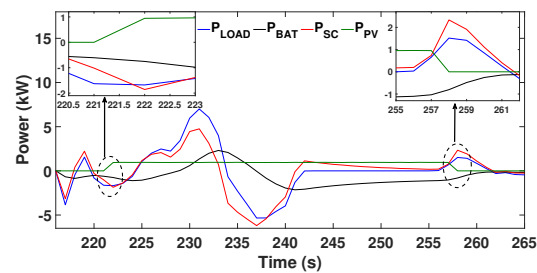


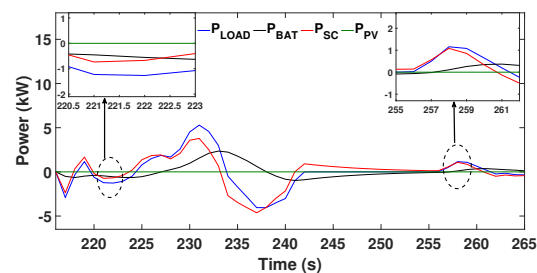
Figure 13. PV energy generation (kWh). (a) Map of selected location for the analysis (Bangalore-12.9716° N, 77.5946° E). (b) PV energy generation (kWh) at Bangalore, India throughout the year.

This section explores varying environmental conditions, such as sudden irradiance change. PV power constantly fluctuates due to the varying irradiance and temperature. An MPPT supports achieving maximum power at each irradiance level. An increase in irradiance from 0 to 1000 W/m² at $t = 221$ s, and a decrease from 1000 to 0 W/m² at $t = 257$ s verify sudden PV power variations. The power allocation of IHSEMS described in Figure 14a includes the load power, battery power, SC power, and PV power. IHSEMS took care of the load demand at $t = 221$ s, where PV irradiance and regenerative braking excess power were at the bus. SC consumed this excess power at that instant by consuming more power (-ve rise shows the sudden increase in SC charge power) to avoid disturbances in battery power. At $t = 257$ s, the PV irradiance suddenly reduced to zero, and traction operation demanded a dip in power at the bus. The SC delivered more power (+ve rise

shows the sudden increase in SC discharge power) to avoid fluctuations in battery power. This strategy ensures a smooth battery operation during rising and falling PV irradiance and load variations. Similarly, Figure 14b shows the same load fluctuation as discussed in Figure 14a. However, the PV power is considered zero to analyze the impact of energy management during the same load fluctuations but with different environmental conditions. Under zero PV irradiance, the SC does not take additional charge or discharge currents as in the case of Figure 14a. Three different driving cases were considered based on the instant of the driving time in a day, and are as follows:



(a) Power comparison with PV irradiance variations.



(b) Power comparison with zero PV irradiance.

Figure 14. Power allocation of IHSEMS for sudden variation in solar irradiance (a) at zero PV power; (b) under NYCC driving cycle.

Case I: Where daily average PV irradiance is available for charging;

Case II: Where half of daily average PV irradiance is available for charging;

Case III: Where zero daily average PV irradiance is available for charging.

In the first case, an average drive of a 3W is 100 km under a full sunshine hour (PV power = full). The driving schedule scenario and energy consumption of the first case are shown in Table 3. An additional 20% energy consumption for varying driving profiles (driver/route/road terrain, etc.) is considered in the analysis. In the second case, an average drive of a 3W is 100 km under a half-sunshine hour (PV power = half). In the third case, an average drive of a 3W is 100 km during night time (PV power = 0).

Table 3 summarizes different cases, and it is clear that when compared with a BEV, a hybrid EV with a PV, battery, and SC can achieve higher vehicle performance and energy efficiency with a lower battery size. Furthermore, case-II was selected for further analysis at a half sunshine hour and a half outside. The half sunshine hour was due to shading obstacles during driving and parking, and variations in seasons may cause losses in irradiance (nearly 60–70% losses) [63]. In order to match the actual scenario, all the environmental and driving conditions are considered in this paper. In tropical countries where irradiance is very high throughout the year, the battery charging from the grid could be reduced. Further, PV could manage the daily commute of the vehicle, and the battery could be used as an emergency source. PV saves time for charging and also shifts the

attitude of EV users who are hesitant to use EVs due to the shortage of EV charging stations and high charging time. In the future, the position of PV power in transportation systems will be high because, according to the Paris Agreement, all countries will reduce their global peaks of greenhouse gas emissions as soon as possible to achieve global climate change by 2050 [6]. A further increase in PV module conversion efficiency and reduction in PV cell cost can improve the EV energy efficiency to a large extent [66].

3.2. Techno-Economic Analysis

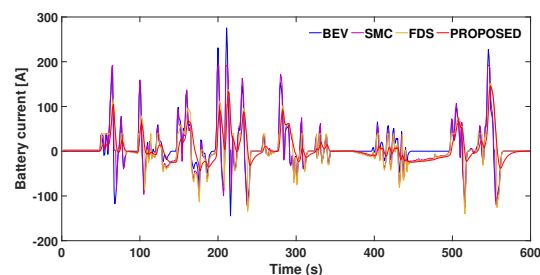
The comparison of technical parameters and economy analysis exhibits the significance of the hybrid-source EMS strategy. Various EMSs strategies:

- (1) IHSEMS;
- (2) SMC [41];
- (3) FDS [42]; and
- (4) BEV

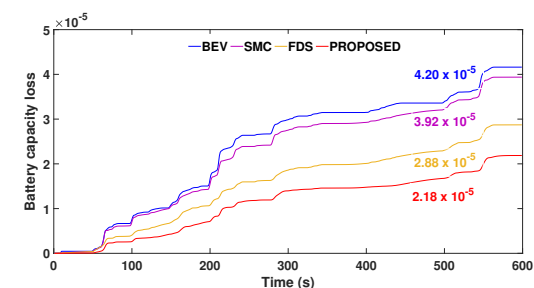
have been evaluated for a fair and guaranteed comparison. The analysis also presents a BEV configuration to highlight the superiority of hybrid-source EVs. An NYCC cycle showed the best urban driving profile, as shown in Figure 4. Therefore, it was selected for technical and economic comparison of EMS [44] below (Sections 3.2.1 and 3.2.2).

3.2.1. Technical Performance Comparison of EMSs

This subsection compares specific performance parameters of BEVs, existing EMS, and proposed EMS. Figure 15 illustrates the battery current and capacity loss performance under the NYCC cycle for three different hybrid EMS. The battery-only (BEV) configuration was also analyzed to illustrate the significance of hybrid sources in EVs. It is clear from Figure 15a that FDS and IHSEMS appear similar. However, FDS failed to reduce the average battery current at $t = 300$ s– 350 s, 400 s– 450 s, and 520 s– 560 s, which eventually reflects in the battery degradation, and the IHSEMS performed better in reducing battery capacity loss than all strategies, as shown in Figure 15b. IHSEMS reduced frequent battery charging events and thus achieved a decelerated battery degradation. Hence, the battery capacity loss was reduced by 48.10% in comparison with the BEV under the NYCC cycle, where the capacity loss is evaluated with Equation (19) and depicted in Section 2.4(e).



(a) Comparison of battery current.



(b) Comparison of battery capacity loss.

Figure 15. Comparison of BEV, SMC, FDS, and IHSEMS in terms of battery current (a) and battery capacity loss (b) under NYCC driving cycle.

Figure 16a,b illustrate two different time intervals for peak load power and sudden fluctuations in the battery power profile. The SC absorbs the transient conditions and prevents the battery from reaching higher C-rates and fluctuations. During the time interval 543 s–549 s in Figure 16a, IHSEMS, SMC, and FDS reduced the respective peak battery power by 50.20%, 48.33%, and 27.12% compared to BEVs as per Equation (14). The effective control of C-rates in peak power instants has been found in the proposed strategy compared to the existing EMS and BEVs. Similarly, as shown in Figure 16b, during the interval $t = 400$ s–440 s, the proposed strategy effectively reduced power fluctuations compared to the other EMS. The BIR, as discussed in Section 2.4(c) and evaluated in Equation (17), reduced to 76.2% for IHSEMS compared to the BEV. Hence, it is evident that battery stresses were minimized. Similarly, during $t = 450$ s–495 s, PV power fluctuations were higher and reflected in the battery power of SMC and FDS strategies. However, the proposed EMS removes the fluctuations, making the battery power profile much smoother and decelerating the battery's degradation. Moreover, RMS current reduction detailed in Section 2.4(d) and expressed in Equation (18) shows the IHSEMS achieved a reduction by 46.60% compared with BEV, 37.88% compared with SMC, and 17.03% compared with FDS.

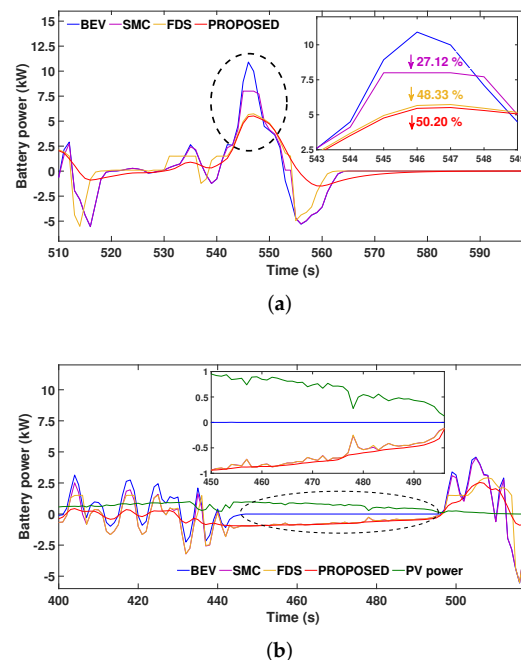


Figure 16. Comparison of BEV, SMC, FDS, and proposed IHSEMS under NYCC driving cycle. (a) Comparison of peak battery power for NYCC driving cycle (510 s–599 s). (b) Comparison of power fluctuations for NYCC driving cycle (400 s–520 s).

The IHSEMS reduces the battery capacity loss and can plan the availability of SC. Figure 17 shows the comparison of SOC of SC under the NYCC cycle for SMC, FDS, and IHSEMS. In NYCC (urban cycle), the IHSEMS initially controlled the SC to utilize maximum and later charges through the battery and braking energy, which was impossible through FDS and SMC EMSs. In the IHSEMS, the final value of SC_{SOC} was maintained at 85% for the smooth operation of (charging and discharging) future driving cycles. Conversely, other EMS charged the SC to its maximum SOC, which increased the battery deterioration. Capacity loss of battery for the NYCC cycle was very low for IHSEMS compared with other EMS, and evaluated as discussed in Section 2.4(e). The performance parameters for BEV, SMC, FDS, and IHSEMS are explained in Table 4. Section 2.4(b) depicts the B_{CR} , evaluated as per Equation (15), which was 26.72% for IHSEMS compared to the BEV. The higher fluctuations in the NYCC driving profile provided an extreme environment for battery degradation and reduced the battery life span. To analyze the battery lifespan for

BEV and hybrid EMSs, repeated NYCC cycles were tested and analyzed. Life span, as discussed in Section 2.4(f), and evaluated using Equation (22), shows that a battery life span improvement (BLSI) of 6.91%, 45.50%, and 92.68% was achieved for the hybrid EMSs SMC, FDS, and proposed IHSEMS, respectively, compared to the BEV (Table 4).

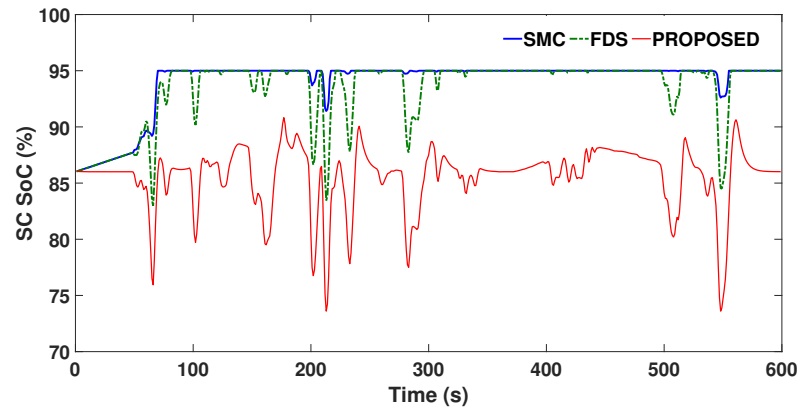


Figure 17. Comparison of SC_{SoC} with SMC, FDS, and IHSEMS under NYCC driving cycle.

The bus voltage constantly fluctuates due to the sudden variations in EV load current. Section 2.4(g) describes the DC_{BVF} adversely affecting EV motor performance. However, the controller brings back the system stability with a fast response. Figure 18 shows the comparison of DC_{BVF} with BEV, SMC, FDS, and IHSEMS under the NYCC cycle. DC_{BVF} of BEV was higher compared to SMC, FDS, and IHSEMS, and was 13.19%, 10.90%, 5.20%, and 2.05%, respectively, as tabulated in Table 4. The proposed EMS reduces the DC_{BVF} as evaluated using Equation (23) by maximum utilization of the SC during sudden load changes. The lower DC_{BVF} (nearly 2%) in IHSEMS highly recommends an efficient motor drive system.

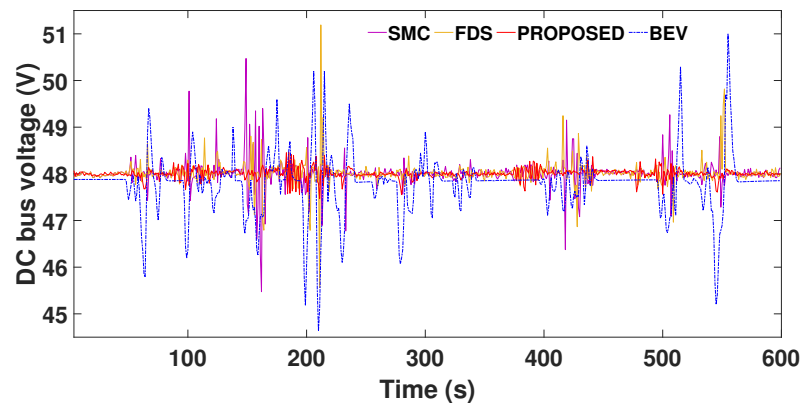


Figure 18. Comparison of DC_{BVF} bus voltage fluctuations with SMC, FDS, and IHSEMS under NYCC driving cycle.

Table 4. Performance and economy analysis of EMS.

Sl no	Parameters	BEV	SMC	FDS	IHSEMS
1	Battery Peak Power (kW)	10.93	7.96	5.64	5.44
2	Battery capacity (kWh)	7.37	5.4	5.4	5.4
3	Battery di/dt (A/s)	113	98	61	26.8
4	Battery RMS current (A)	64	54.95	41.14	34.13
5	Battery Capacity Loss	4.20×10^{-5}	3.92×10^{-5}	2.88×10^{-5}	2.18×10^{-5}
6	Battery Life Span Improvement (%)	-	6.91%	45.50%	92.68%
7	DC bus voltage fluctuations (%)	13.19%	10.40%	5.20%	2.05%
8	Total Operational Cost (INR.)	18.54	12.942	9.50	7.25

3.2.2. Economy Analysis of EMSs

The battery's technical parameters reflect the impact on economic analysis, as discussed in Section 3.2.1. Section 2.5(c)–(a) estimates the total operation cost (TOC), including the sum of electricity cost (EC) and battery degradation cost (BDC) of the EV. Figure 19 illustrates the comparative results of EC, BDC, and TOC of the SMC, FDS, BEV, and IHSEMS for a 100 km drive. The proposed IHSEMS reduces the electricity cost by 52.4% (INR. 17.31/100 km) compared to the BEV. Moreover, BEV experiences a higher battery degradation cost and, in turn, a higher chance of replacement or maintenance. Comparison of economic analysis, in terms of TOC, is included in Table 4. Compared to the BEV, SMC, and FDS, the IHSEMS strategy reduces the total operation cost by 60%, 43.9%, and 23.68%, respectively.

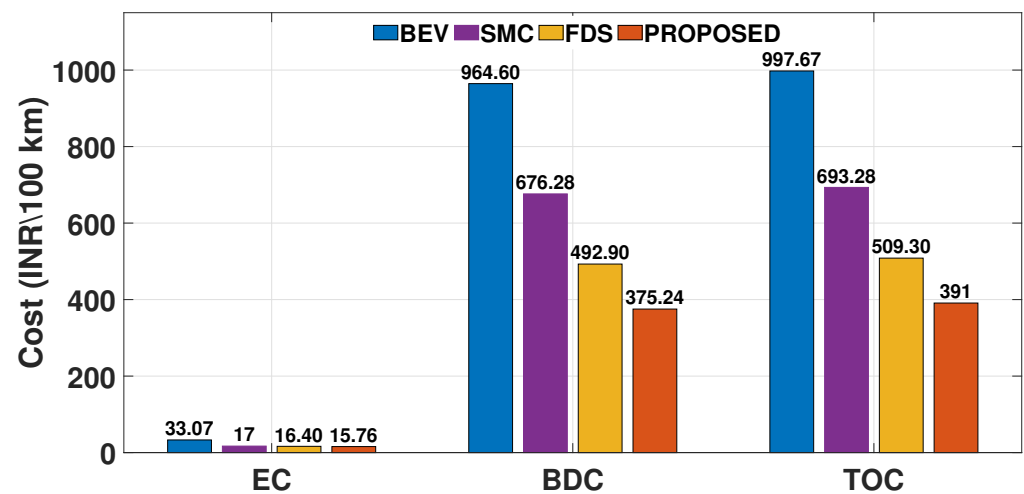


Figure 19. Economic analysis of EV with SMC, FDS, BEV, and IHSEMS.

4. Conclusions

Globally, a sustainable economy depends on the rapid development of renewable energy applications. In this context, a hybrid source with a renewable background plays a crucial position in the transportation sector. The present work highlights the importance of EMS for hybrid-source EVs with design and simulation modelling. The proposed IHSEMS allocates the load power to enhance the performance of the EV. The IHSEMS effectively manages the effects of varying driving conditions by employing an absolute energy-sharing strategy. Incorporating solar and supercapacitors with existing BEVs improves battery life and energy efficiency. The SMC and FDS strategies were analyzed in the comparative study. Significant contributions and highlights of the proposed EMS are:

- The battery's stress reduces in IHSEMS by reducing RMS current by 46.60%, 37.88%, and 17.03% compared with BEV, SMC, and FDS methods.
- The battery peak power reduces in IHSEMS by 50.2%, 30.74%, and 3.71% compared with BEV, SMC, and FDS methods.
- Compared to BEV, the battery capacity reduces in IHSEMS by 26.72% (7.37 kWh to 5.4 kWh).
- The IHSEMS exhibits a reduction in battery peak power, RMS current, and continuous charge–discharge cycles, which improves the battery lifespan by 92.68%, 80.22%, and 32.40% compared with BEV, SMC, and FDS EMS, respectively.
- Economic analysis of IHSEMS shows a reduction of 60%, 43.9%, and 23.68% in total operation cost compared to BEV, SMC, and FDS, respectively.

The next step of this study includes the extension of the proposed methodology into larger vehicles to highlight the PV's capabilities to adequately cover the modern BEV's energy needs under normal consumption conditions (200–300 km per week) [67]. The key to the success of such a solution is the combination of eco-friendly driving behavior (e.g., smooth accelerations and decelerations, low average speeds, daytime driving, parking, and charging outdoors) with the use of marginally sufficient electric motors for the actual transportation needs, which require a fundamental change of the current automotive industry's way of marketing and thinking.

Author Contributions: Conceptualisation, methodology, interviewing, formal analysis, data curation, writing—original draft preparation, V.P.S.; methodology, writing—review and editing, supervision, Y.K.; investigation, writing—review and editing, funding acquisition, supervision, P.K. All authors have read and agreed to the published version of the manuscript.

Funding: This research received no external funding.

Data Availability Statement: Not applicable.

Acknowledgments: P.K. acknowledges the Eiffel project under grant agreement 101003518.

Conflicts of Interest: The authors declare no conflict of interest.

Abbreviations

BEV	Battery Electric vehicles
BMS	Battery management systems
DP	Dynamic programming
ECMS	Equivalent consumption minimization strategy
EV	Electric vehicle
EM	Energy Management
EMS	Energy management strategies
FCEV	Fuel cell electric vehicles
GA	Genetic algorithm
HSEV	Hybrid source electric vehicles
IHSEMS	Intelligent Hybrid Source Energy Management Strategy
MPC	Model predictive control
NDC	Nationally Determined Contribution
NYCC	New York city cycle
PSO	Particle swarm optimization
PV	Photovoltaic
RMS	Root mean square
STEPS	Stated Policies Scenario
SC	Supercapacitor
SDS	Sustainable Development Scenario
3W	Three-wheeler
WLTP	Worldwide Harmonized Light Vehicles Test Procedure

References

1. International Energy Agency. Outlook for Biogas and Biomethane: Prospects for Organic Growth 2020. Available online: <https://www.iea.org/reports/outlook-for-biogas-and-biomethane-prospects-for-organic-growth> (accessed on 12 January 2022).
2. International Energy Agency. World Energy Outlook 2021. Available online: <https://www.iea.org/reports/india-energy-outlook-2021> (accessed on 18 May 2022).
3. International Energy Agency. India Energy Outlook 2021. Available online: <https://www.iea.org/reports/india-energy-outlook-2021/energy-in-india-today> (accessed on 25 April 2022).
4. Jia, L.; Ma, J.; Cheng, P.; Liu, Y. A perspective on solar energy-powered road and rail transportation in China. *J. Power Energy Syst.* **2021**, *6*, 760–771.
5. International Renewable Energy Agency. Global Energy Transformation: A Roadmap to 2050 (2019 Edition). 2019. Available online: <https://www.irena.org/publications/2019/Apr/Global-energytransformation-a-roadmap-to-2050> (accessed on 15 April 2021).

6. Resources for the Future. (2020, May). Global Energy Outlook 2020: Energy Transition or Energy Addition? Available online: <https://www.rff.org/publications/reports/global-energy-outlook-2020> (accessed on 22 May 2021).
7. Goel, S.; Sharma, R.; Rathore, A.K. A review on barrier and challenges of electric vehicle in India and vehicle to grid optimisation. *Transp. Eng.* **2021**, *4*, 1–14. [[CrossRef](#)]
8. The Oil and Gas Industry in Energy Transitions. Available online: <https://www.iea.org/reports/the-oil-and-gas-industry-in-energy-transitions> (accessed on 10 November 2021).
9. Peter, R.; Gregor, K.; Timur, G.; Wolfgang, S.; Janusz, C.; Zbigniew, K.; Pallav, P.; Chris, H.; Markus, A.; Jens, B.-K.; et al. Outlook for clean air in the context of sustainable development goals. *Glob. Environ. Chang.* **2018**, *53*, 1–11.
10. Agrawal, R.C.; Pandey, G.P. Solid polymer electrolytes: Materials designing and all-solid-state battery applications: An overview. *J. Phys. D Appl. Phys.* **2008**, *41*, 1–18. [[CrossRef](#)]
11. Andwari, A.M.; Pesiridis, A.; Rajoo, S. A review of Battery Electric Vehicle technology and readiness levels. *Renew. Sustain. Energy Rev.* **2017**, *78*, 414–430. [[CrossRef](#)]
12. Schuster, S.F.; Brand, M.J.; Berg, P.; Gleissenberger, M. Lithium-ion cell-to-cell variation during battery electric vehicle operation. *J. Power Sources* **2017**, *297*, 242–251. [[CrossRef](#)]
13. Marques, P.; Garcia, R.; Kulay, L.; Freire, F. Comparative life cycle assessment of lithium-ion batteries for electric vehicles addressing capacity fade. *J. Clean. Prod.* **2019**, *229*, 787–794. [[CrossRef](#)]
14. Zhang, J.; Wang, Z.; Liu, P.; Zhang, Z. Energy consumption analysis and prediction of electric vehicles based on real-world driving data. *Appl. Energy* **2020**, *275*, 1–15. [[CrossRef](#)]
15. Bonfiglio, C.; Roessler, W. A cost optimized battery management system with active cell balancing for lithium ion battery stacks. *IEEE Veh. Power Propuls. Conf.* **2009**, *275*, 304–309.
16. Sun, L.; Feng, K.; Chapman, C.; Zhang, N. An Adaptive Power-Split Strategy for Battery–Supercapacitor Powertrain—Design, Simulation, and Experiment. *IEEE Trans. Power Electron.* **2017**, *32*, 9364–9375. [[CrossRef](#)]
17. Panaparambil, V.S.; Kashyap, Y. A review on hybrid source energy management strategies for electric vehicle. *Int. J. Energy Res.* **2021**, *45*, 19819–19850. [[CrossRef](#)]
18. Xie, J.; Yang, P.; Wang, Y.; Qi, T.; Lei, Y.; Li, C.M. Puzzles and confusions in supercapacitor and battery: Theory and solutions. *J. Power Sources* **2018**, *401*, 213–223. [[CrossRef](#)]
19. Snoussi, J.; Ben Elghali, S.; Benbouzid, M.; Mimouni, M. Auto-adaptive filtering-based energy management strategy for fuel cell hybrid electric vehicles. *Energies* **2018**, *11*, 2118. [[CrossRef](#)]
20. Li, H.; Ravey, A.; N'Diaye, A.; Djerdir, A. Online adaptive equivalent consumption minimization strategy for fuel cell hybrid electric vehicle considering power sources degradation. *Energy Convers. Manag.* **2019**, *192*, 133–149. [[CrossRef](#)]
21. Solar Photovoltaic Power Potential by Country. Available online: <https://www.worldbank.org/en/topic/energy/publication/solar-photovoltaic-power-potential-by-country> (accessed on 13 January 2021).
22. Kouchachvili, L.; Yaïci, W.; Entchev, E. Hybrid battery/supercapacitor energy storage system for the electric vehicles. *J. Power Sources* **2018**, *374*, 237–248. [[CrossRef](#)]
23. Wen, H.; Xiao, W.; Li, H.; Wen, X. Analysis and minimisation of DC bus surge voltage for electric vehicle applications. *IET Electr. Syst. Transp.* **2012**, *2*, 68–76. [[CrossRef](#)]
24. Nguyen, H.-L.T.; Nguyễn, B.-H.; Vo-Duy, T.; Trovão, J.P.F. A Comparative Study of Adaptive Filtering Strategies for Hybrid Energy Storage Systems in Electric Vehicles. *Energies* **2021**, *14*, 3373. [[CrossRef](#)]
25. Vargas, U.; Lazaroiu, G.C.; Tironi, E.; Ramirez, A. Harmonic modeling and simulation of a stand-alone photovoltaic-battery-supercapacitor hybrid system. *Int. J. Electr. Power Energy Syst.* **2019**, *105*, 70–78. [[CrossRef](#)]
26. Kumar, P.; Roy, S.; Karayaka, H.B.; Yan, Y.; Alqudah, Y. Investigations into best cost battery-supercapacitor hybrid energy storage system for a utility scale PV array. *J. Energy Storage* **2019**, *22*, 150–159.
27. Cabrane, Z.; Kim, J.; Yoo, K.; Ouassaid, M. HESS-based photovoltaic/batteries/supercapacitors: Energy management strategy and DC bus voltage stabilization. *Sol. Energy* **2021**, *216*, 551–563. [[CrossRef](#)]
28. Armenta, J.; Núñez, C.; Visairo, N.; Lázaro, I. An advanced energy management system for controlling the ultracapacitor discharge and improving the electric vehicle range. *J. Power Sources* **2015**, *56*, 452–458. [[CrossRef](#)]
29. Blanes, J.M.; Gutiérrez, R.; Garrigós, A.; Lizán, J.L.; Cuadrado, J.M. Electric Vehicle Battery Life Extension Using Ultracapacitors and an FPGA Controlled Interleaved Buck–Boost Converter. *IEEE Trans. Power Electron.* **2013**, *28*, 5940–5948. [[CrossRef](#)]
30. Demircali, A.; Koroglu, S. Modular energy management system with Jaya algorithm for hybrid energy storage in electric vehicles. *Int. J. Energy Res.* **2022**, *28*, 1–14. [[CrossRef](#)]
31. Abeywardana, D.B.W.; Hredzak, B.; Agelidis, V.G.; Demetriades, G.D. Supercapacitor Sizing Method for Energy-Controlled Filter-Based Hybrid Energy Storage Systems. *IEEE Trans. Power Electron.* **2017**, *32*, 1626–1637. [[CrossRef](#)]
32. Castaigns, A.; Lhomme, W.; Trigui, R.; Bouscayrol, A. Comparison of energy management strategies of a battery/supercapacitors system for electric vehicle under real-time constraints. *Appl. Energy* **2016**, *163*, 190–200. [[CrossRef](#)]
33. Florescu, A.; Bacha, S.; Munteanu, I.; Bratcu, A.I.; Rumeau, A. Adaptive frequency separation-based energy management system for electric vehicles. *J. Power Sources* **2015**, *280*, 410–421. [[CrossRef](#)]
34. Zhang, F.; Wang, L.; Coskun, S.; Pang, H.; Cui, Y.; Xi, J. Energy Management Strategies for Hybrid Electric Vehicles: Review, Classification, Comparison, and Outlook. *Energies* **2020**, *13*, 3352. [[CrossRef](#)]

35. Chen, Z.; Xiong, R.; Cao, J. Particle swarm optimization-based optimal power management of plug-in hybrid electric vehicles considering uncertain driving conditions. *Energy* **2015**, *96*, 197–208. [CrossRef]
36. Wiecezorek, M.; Lewandowski, M. A mathematical representation of an energy management strategy for hybrid energy storage system in electric vehicle and real time optimization using a genetic algorithm. *Appl. Energy* **2017**, *192*, 222–233. [CrossRef]
37. Li, H.; Ravey, A.; N'Diaye, A.; Djerdir, A. Equivalent consumption minimization strategy for fuel cell hybrid electric vehicle considering fuel cell degradation. In Proceedings of the IEEE Transportation Electrification Conference and Expo (ITEC), Chicago, IL, USA, 22–24 June 2017; pp. 540–544.
38. Zhou, F.; Xiao, F.; Chang, C.; Shao, Y.; Song, C. Adaptive model predictive control-based energy management for semi-active hybrid energy storage systems on electric vehicles. *Energies* **2017**, *10*, 1063. [CrossRef]
39. Sellali, M.; Abdeddaim, S.; Betka, A.; Djerdir, A.; Drid, S.; Tiar, M. Fuzzy-Super twisting control implementation of battery/super capacitor for electric vehicles. *ISA Trans.* **2019**, *95*, 243–253. [CrossRef] [PubMed]
40. Trovão, J.P.F.; Roux, M.; Ménard, É.; Dubois, M.R. Energy- and Power-Split Management of Dual Energy Storage System for a Three-Wheel Electric Vehicle. *IEEE Trans. Veh. Technol.* **2017**, *66*, 5540–5550. [CrossRef]
41. Njoya Motapon, S.; Dessaint, L.A.; Al-Haddad, K. A Comparative Study of Energy Management Schemes for a Fuel-Cell Hybrid Emergency Power System of More-Electric Aircraft. *IEEE Trans. Ind. Electron.* **2014**, *61*, 1320–1334. [CrossRef]
42. Cabrane, Z.; Batoool, D.; Kim, J.; Yoo, K. Design and simulation studies of battery-supercapacitor hybrid energy storage system for improved performances of traction system of solar vehicle. *J. Energy Storage* **2020**, *32*, 5540–5550. [CrossRef]
43. Vukajlović, N.; Milićević, D.; Dumnić, B.; Popadić, B. Comparative analysis of the supercapacitor influence on lithium battery cycle life in electric vehicle energy storage. *J. Energy Storage* **2020**, *31*, 101603. [CrossRef]
44. Niu, J.; Zhuang, W.; Ye, J.; Song, Z.; Yin, G.; Zhang, Y. Optimal sizing and learning-based energy management strategy of NCR/LTO hybrid battery system for electric taxis. *Energy* **2022**, *257*, 124653. [CrossRef]
45. NPTEL: 2020. Available online: <https://nptel.ac.in/courses/108/103/108103009/> (accessed on 6 May 2021).
46. USEP-Agency. Dynamometer Drive Schedules. 4.1. 2022. Available online: <https://www.epa.gov/vehicle-and-fuel-emissions-testing/dynamometer-drive-schedule> (accessed on 5 October 2022).
47. Mellincovsky, M.; Kuperman, A.; Lerman, C.; Gadelovits, S.; Aharon, I.; Reichbach, N. Performance and limitations of a constant power-fed supercapacitor. *IEEE Trans. Energy Convers* **2014**, *3*, 191–200.
48. Raman, S.R.; Cheng, K.-W.; Xue, X.-D.; Fong, Y.-C.; Cheung, S. Hybrid Energy Storage System with Vehicle Body Integrated Super-Capacitor and Li-Ion Battery: Model, Design and Implementation, for Distributed Energy Storage. *Energies* **2021**, *14*, 6553. [CrossRef]
49. Sunrunmotors. 2022. Available online: <http://www.sunrunmotors.com/> (accessed on 2 November 2022).
50. Wang, C.; Liu, R.; Tang, A. Energy management strategy of hybrid energy storage system for electric vehicles based on genetic algorithm optimization and temperature effect. *J. Energy Storage* **2022**, *51*, 104314. [CrossRef]
51. Erickson, R.W. Maksimovic, Controller Design. In *D. Fundamentals of Power Electronics*; Springer: Berlin, Germany, 2020; pp. 347–405.
52. Samad, N.A.; Kim, Y.; Siegel, J.B.; Stefanopoulou, A.G. Influence of Battery Downsizing and SOC Operating Window on Battery Pack Performance in a Hybrid Electric Vehicle. In Proceedings of the IEEE Vehicle Power and Propulsion Conference (VPPC), Montreal, QC, Canada, 19–22 October 2015; pp. 1–6.
53. Xiong, R.; Pan, Y.; Shen, W.; Li, H.; Sun, F. Lithium-ion battery aging mechanisms and diagnosis method for automotive applications: Recent advances and perspectives. *Renew. Sustain. Energy Rev.* **2020**, *131*, 110048. [CrossRef]
54. Jangid, M.K.; Mukhopadhyay, A.; Mater, J. Real-time monitoring of stress development during electrochemical cycling of electrode materials for Li-ion batteries: Overview and perspectives. *Chem. A* **2019**, *7*, 23679–23726. [CrossRef]
55. Hussain, S.; Ali, M.U.; Park, G.S.; Nengroo, S.H.; Khan, M.A.; Kim, H.J. A Real-Time Bi-Adaptive Controller-Based Energy Management System for Battery-Supercapacitor Hybrid Electric Vehicles. *Energies* **2019**, *12*, 4662. [CrossRef]
56. Song, Z.; Li, J.; Hou, J.; Hofmann, H.; Ouyang, M.; Du, J. The battery-supercapacitor hybrid energy storage system in electric vehicle applications: A case study. *Energy* **2018**, *154*, 433–441. [CrossRef]
57. BloombergNEF. Hitting the EV Inflection Point. 2021. Available online: <https://www.transportenvironment.org/discover/hitting-the-ev-inflection-point/> (accessed on 2 January 2022).
58. Wang, J.; Liu, P.; Hicks-Garner, J.; Sherman, E.; Soukiazian, S.; Verbrugge, M.; Tataria, H.; Musser, J.; Finamore, P. Cycle-life model for graphite-LiFePO₄ cells. *J. Power Sources* **2011**, *196*, 3942–3948. [CrossRef]
59. Guide to EV Adoption. Available online: <https://www.wbcds.org/Programs/Cities-and-Mobility/Transforming-Urban-Mobility/Mobility-Decarbonization/Coalitions/Resources/India-Business-Guide-to-EV-Adoption> (accessed on 15 May 2020).
60. Spotnitz, R. Simulation of capacity fade in lithium-ion batteries. *J. Power Sources* **2003**, *113*, 72–80. [CrossRef]
61. Huang, J.; Huang, Z.; Wu, Y.; Liu, Y.; Li, H.; Jiang, F.; Peng, J. Sizing optimization research considering mass effect of hybrid energy storage system in electric vehicles. *J. Energy Storage* **2022**, *48*, 103892. [CrossRef]
62. Akar, F.; Tavlasoglu, Y.; Vural, B. An Energy Management Strategy for a Concept Battery/Supercapacitor Electric Vehicle With Improved Battery Life. *IEEE Trans. Transp. Electrification* **2016**, *3*, 191–200. [CrossRef]
63. Sagaria, S.; Duarte, G.; Neves, D.; Baptista, P. Photovoltaic integrated electric vehicles: Assessment of synergies between solar energy, vehicle types and usage patterns. *J. Clean. Prod.* **2022**, *348*, 131402. [CrossRef]

64. European, Commission. Photovoltaic Geographical Information System. Available online: <https://ec.europa.eu/jrc/en/pvgis> (accessed on 30 January 2015).
65. Brito, M.C.; Santos, T.; Moura, F.; Pera, D.; Rocha, J. Urban solar potential for vehicle integrated photovoltaics. *Transp. Res. Part D Transp. Environ.* **2021**, *94*, 102810. [[CrossRef](#)]
66. Elia, A.; Kamidelivand, M.; Rogan, F.; Gallachóir, B.Ó. Impacts of innovation on renewable energy technology cost reductions. *Renew. Sustain. Energy Rev.* **2022**, *138*, 110488. [[CrossRef](#)]
67. Lightyear. 2022. Available online: <https://lightyear.one/> (accessed on 10 August 2022).

Disclaimer/Publisher's Note: The statements, opinions and data contained in all publications are solely those of the individual author(s) and contributor(s) and not of MDPI and/or the editor(s). MDPI and/or the editor(s) disclaim responsibility for any injury to people or property resulting from any ideas, methods, instructions or products referred to in the content.